Three-dimensional pore-scale modeling of fracture evolution in heterogeneous carbonate caprock subjected to CO_2-enriched brine

Hossein Fazeli[1*], *Ravi A. Patel*[2], *Brian R. Ellis*[3], *Helge Hellevang*[1]

[1]Department of Geosciences, University of Oslo, Pb. 1047, Blindern, Oslo, Norway

[2]Laboratory for waste management (LES), Paul Scherrer Institute, CH-5232, Villigen-PSI, Switzerland

[3]Department of Civil and Environmental Engineering, University of Michigan, Ann Arbor, MI 48109, USA

This document is the accepted manuscript version of the following article:

Fazeli, H., Patel, R. A., Ellis, B. R., & Hellevang, H. (2019). Three-dimensional pore-scale modeling of fracture evolution in heterogeneous carbonate caprock subjected to CO2-enriched brine. Environmental Science and Technology, 53(8), 4630-4639. https://doi.org/10.1021/acs.est.8b05653

Abstract

Fractures in caprocks overlying CO_2 storage reservoirs can adversely impact the sealing capacity of the rocks. Interactions between acidified fluid and minerals with different reactivities along a fracture pathway can affect the chemically-induced changes in hydrodynamic properties of fractures. To study porosity and permeability evolution of small scale (millimeter scale) fractures, a three dimensional pore-scale reactive transport model based on the Lattice Boltzmann method has been developed. The model simulates the evolution of two different fractured carbonate rich caprock samples subjected to flow of CO_2-rich brine. Results show that the existence of nonreactive minerals along the flow path can restrict the increase in permeability and the cubic law used to relate porosity and permeability in mono-mineral fractured systems is therefore not valid in multi-mineral systems. Moreover, injection of CO_2-acidified brine at high rates, resulted in a more permeable fractured media compared to the case with lower injection rates. The overall rate of calcite dissolution along the fracture decreased over time, confirming similar observations from previous continuum scale models. The presented 3D pore-scale model can be used to provide inputs for continuum scale models, such as improved porosity-permeability relationships for heterogeneous rocks, and also to investigate other reactive transport processes in the context of CO_2 leakage in fractured seals.

1. Introduction

CO_2 storage in geological formations is considered to be a viable option to mitigate anthropogenic carbon emissions and will likely be a component of any large-scale strategy to slow the rate of global warming.[1-2] Once injected into a geological formation, CO_2 will move upwards due to buoyancy and there must therefore be a low permeability caprock to prevent CO_2

leakage to the surface[3]. Pre-existing fractures in the caprock or fractures that might form due to the injection of large amount of CO_2 may serve as primary pathways for CO_2 leakage and negatively impact the sealing capacity of the caprock[4-7]. When CO_2-acidified brine is flowing through these fractures, the fracture hydrodynamic properties will change as a result of CO_2-water-rock interactions[8-9]. Modelling of these interactions together with other coupled processes such as fluid flow can enable us to predict the evolution of fracture permeability and, on a larger scale, caprock integrity[10]. There have been different numerical models developed to study mineral dissolution in fractured rocks[11-20]. Some models were designed to evaluate the effect of fluid transport and reactions on the pattern of fracture evolution and channel formation where only one single mineral was present in the rock. The results showed that at high Peclet (Pe) numbers (relative magnitude of advective transport to diffusive transport), more channels will form, whereas low Pe numbers lead to less channeling and a more uniform dissolution front[14, 17-18]. It has furthermore been shown that dissolution will not be spatially uniform for high Damkohler (Da) numbers (relative magnitude of reaction to transport) and that increased fracture roughness can favor channelization [16-17, 19]. It has also been reported that the fracture porosity evolution is more localized near the flow inlet at high Da numbers, while porosity evolution is uniform along the fracture for low Da numbers[11-12, 16]. These studies have focused on single mineral systems, however, evolution of fracture permeability and morphology may also be dependent on the spatial distribution of minerals when minerals with different reactivities are present in the same system[7, 21].

It has been shown that preferential dissolution of fast-reacting minerals (while nonreactive minerals are also present in the rock) can create a porous zone around the main fracture where this zone can suppress the permeability enhancement and decrease the overall reaction rate in the

regions near the fracture[21-22]. To predict the fracture evolution behavior in multimineral systems, there is a need to have predictive numerical models. In this regard, a few continuum scale models have been developed to model the effect of this altered layer around a fracture. Deng et al.[6, 23-24], in a series of work, developed a reduced dimension model and also took into account the erosion and detachment of less/nonreactive minerals. Their model was able to predict the experimental observations indicating that the overall reaction rate is decreasing with time in the altered layer[23]. Recently, Spokas et al.[25] investigated effect of rock mineralogy on reactive fracture evolution using a 2D numerical model which was able to take into account the mechanical deformation. They used the model for different rock mineralogies with different calcite content and their results showed that a banded mineral pattern results in more stabilized transmissivity[25]. The understanding of effects of mineral heterogeneity on the evolution of porous media and reactive fractures can be further improved using pore-scale models that can resolve relevant processes at the microscopic to mm scales[26-28].

Several pore-scale models have been developed to try to capture the effect of co-existence of minerals with different reactivities on the fracture evolution[29-30]. Molins et al.[30] developed a 2D pore-scale model and reproduced the nonuniform aperture increase, as observed by Ellis et al.[7], of a single fracture in a mineralogically heterogeneous rock. Also, Chen et al.[29] investigated the permeability evolution of a single 2D fracture in a synthetic binary mineral system.

In this study, we developed a 3D pore-scale reactive transport model based on the Lattice Boltzmann Method (LBM) to simulate mineral dissolution along a fracture in a carbonate rich rock. The model uses the geochemical solver IPHREEQC[31] to compute source-sink terms due to chemical reaction. The use of IPHREEQC provides added flexibility in terms of accounting for complex reaction networks and allows use of more realistic geochemical reaction rates. To

simulate more realistic fracture systems, two different fracture geometries were extracted from X-ray computed tomography data of a fractured rock composed of a mixture of calcite and other nonreactive minerals. We also investigated how the reactive fractures evolved under different influent flow rates. The pore-scale model also allowed for the study of mass transfer between the rock matrix and fracture inside the calcite depleted zone. Finally, since the model is able to track the evolution of fracture geometry due to dissolution, it was used to evaluate the relationship between porosity and permeability in mineralogically heterogeneous dissolving fractures.

2. Methods

2.1.Input geometry for simulations

The input geometries used in this study were taken from one of the X-ray computed tomography (XCT) scanning experiments performed by Ellis et al.[7, 12]. The rock core was from the Amherstburg limestone in northern Michigan, which is a carbonate rich caprock (calcite content ~50%)[10] used for pilot scale CO_2 injection.[32] Ellis and Peters[10] developed a method to map the 3D distribution of calcite content in the core sample by combining XCT and scanning electron microscopy data. The main focus of this prior work was to determine spatial distribution of calcite since it is a fast-reacting mineral that can be abundant in caprock formations and therefore its dissolution can significantly affect the evolution of caprock fractures[33]. To simulate the fracture geometry evolution under different conditions, two different areas of the full 3D geometry were selected: One area with high calcite content and another with low calcite content but similar fracture aperture characteristics. The dimensions of theses geometries are 2.16 mm × 2.16 mm × 2.16 mm with a grid resolution of 27 μm. The fracture aperture map, the calcite content and the selected areas are displayed in Figure S3.

2.2.Model description

To simulate evolution of the fractured carbonate caprock samples, we needed to solve the governing equations describing fluid flow, chemical species transport and both homogeneous and heterogeneous reactions. Moreover, since our objective was to investigate the effect of dissolution on the hydrodynamic properties of fracture, the model must also take into account the evolution of the rock geometry as the rock is dissolving. In this study, we used a pore-scale LBM based reactive transport model developed by Patel et al. (2014)[34] where they simulated the reaction-diffusion processes including equilibrium reactions. All geochemical calculations are done using IPHREEQC geochemical code, which is coupled with the LBM transport solver. This model was further extended to include the fluid flow solver and also validated with the kinetic reactions in a previous study[35]. In the present work, we employ the 3D version of the model in order to capture fracture dissolution and fluid transport within a 3D pore network. Further details regarding the model development and approach are available in the Supporting Information (SI).

In our 3D simulations, CO_2-rich brine was injected through the fracture. The brine initially present in the fracture was assumed to be in equilibrium with the calcite minerals in the system while the injected brine had a pH of around 4.6 and was undersaturated with respect to calcite with a saturation index of around -0.9 (the brine compositions are listed in Table S1). The viscosity of brine was 10^{-3} Pa.s and diffusion coefficients of all chemical species were equal to $2x10^{-9}$ m^2/s. In all numerical experiments fluid flow was driven using a constant pressure gradient across the sample and for each geometry, two different pressure gradients (10 $Pa.m^{-1}$ and 0.1 $Pa.m^{-1}$) were applied in order to investigate the effect of different flow rates on the fracture alteration. For the geometry with high calcite content these pressure gradients result in Peclet (Pe) numbers of 0.019 and 1.9 corresponding to the lower and higher pressure gradients,

respectively. Also, the Pe numbers for the geometry with low calcite content are 0.017 and 1.7 for the higher and lower pressure gradients, respectively. The Pe number is defined as $Pe = \frac{u_{avg}.b}{D}$ where u_{avg} is average pore velocity, b is characteristic length which is considered to be the mean fracture aperture and D is diffusion coefficient. These parameters together with initial porosity and permeability of the input geometries are listed in Table S2.

As previously discussed, the CT scan data used in this study did not determine full 3D mineralogy of the core but instead just separated minerals into either calcite or non-calcite groupings. The non-calcite minerals include dolomite, quartz, fluorite, clay minerals and anhydrite[10]. The dolomite amounts to 30%wt of the core plug and the other non-calcite minerals constitute 20%wt of total mineral content[10]. Since the non-calcite minerals are not differentiated throughout the sample including regions 1 and 2 in Figure S3, they are here simply treated as the nonreactive minerals relative to calcite. This is a fair assumption because according to the reported kinetic data for different minerals, the rate constant for calcite dissolution is an order of magnitude larger than dolomite's rate constant and orders of magnitude larger than that of other minerals[33, 36]. Therefore, the non-calcite minerals can be regarded as nonreactive given the time scale of the simulations performed in this work. For reservoir scale simulations or for longer simulation times, however, kinetics of dolomite and other slow reacting minerals can be added to the model.

Calcite is assumed to react according to the following reaction pathways[37-38]

$$CaCO_{3(s)} + H^+ \rightleftharpoons Ca^{2+} + HCO_3^- \quad (1a)$$

$$CaCO_{3(s)} + H_2CO_3^* \rightleftharpoons Ca^{2+} + 2HCO_3^- \quad (1b)$$

$$CaCO_{3(s)} \rightleftharpoons Ca^{2+} + CO_3^{2-} \quad (1c)$$

and the reaction rate is described by[30]

$$R_{CaCO_3} = (k_1 a_{H^+} + k_2 a_{H_2CO_3^*} + k_3)(1 - \frac{a_{Ca^{2+}} a_{CO_3^{2-}}}{K_{eq,CaCO_3}}) \quad (2)$$

Where a_i is activity of species i, R_{CaCO_3} is reaction rate, k_1, k_2 and k_3 are reaction rate constants which are equal to 0.89, 5.01×10^{-4} and 6.6×10^{-7} mol/(m^2.s), respectively. The equilibrium constant of the reaction ($K_{eq,CaCO_3}$) in Equation (2) is equal to $10^{-8.49}$. The equilibrium and reaction rate constants are related to 25 ºC.

In the following sections we study how fractures evolve under different flow conditions and how the presence of nonreactive minerals along a fracture pathway affects the bulk reaction rate of calcite. Finally, we investigate the fracture evolution by measuring porosity and permeability of the fractured media.

3. Results and Discussion

3.1. Fracture evolution pattern

When CO_2-enriched brine flows through the fracture, it dissolves calcite and causes an increase in local fracture aperture. Figure 1 shows the Ca concentration (mol/L) profiles at t = 0.01 hr, t = 2.6 hr, and t = 7.6 hr for the geometry with high calcite content. In these figures, the light gray is referring to the nonreactive minerals and the red color is representing calcite. Two different cases have been considered to also investigate how the velocity of the influent can affect the fracture evolution. The upper panel in Figure 1 corresponds to the case with lower velocity when the initial Pe number (before reaction) is 0.019 and the lower panel is for the case with an initial Pe number (before reaction) of 1.9. As it can be seen in Figure 1, when Pe number is higher the fluid has a shorter residence time and remains at low pH conditions far from calcite equilibrium. This causes the aperture to increase uniformly along the entire fracture plane. However, when the acidic solution is flowing more slowly, calcite dissolution occurs near the fluid inlet and the

acidic solution only affects the areas around the inlet and the remaining parts of the fracture are unaffected by calcite dissolution. The difference in calcite dissolution, between higher and lower velocity cases, can be better observed at t=7.6 hr in Figure 1.

The same fracture evolution patterns are observed in the case of low calcite content geometries (Figure 2). Higher fluid velocity promotes greater calcite dissolution along the fracture plane but since calcite is less abundant in this scenario the difference in fracture evolutions between the higher and lower velocity cases is not as clear as in models with higher calcite content.

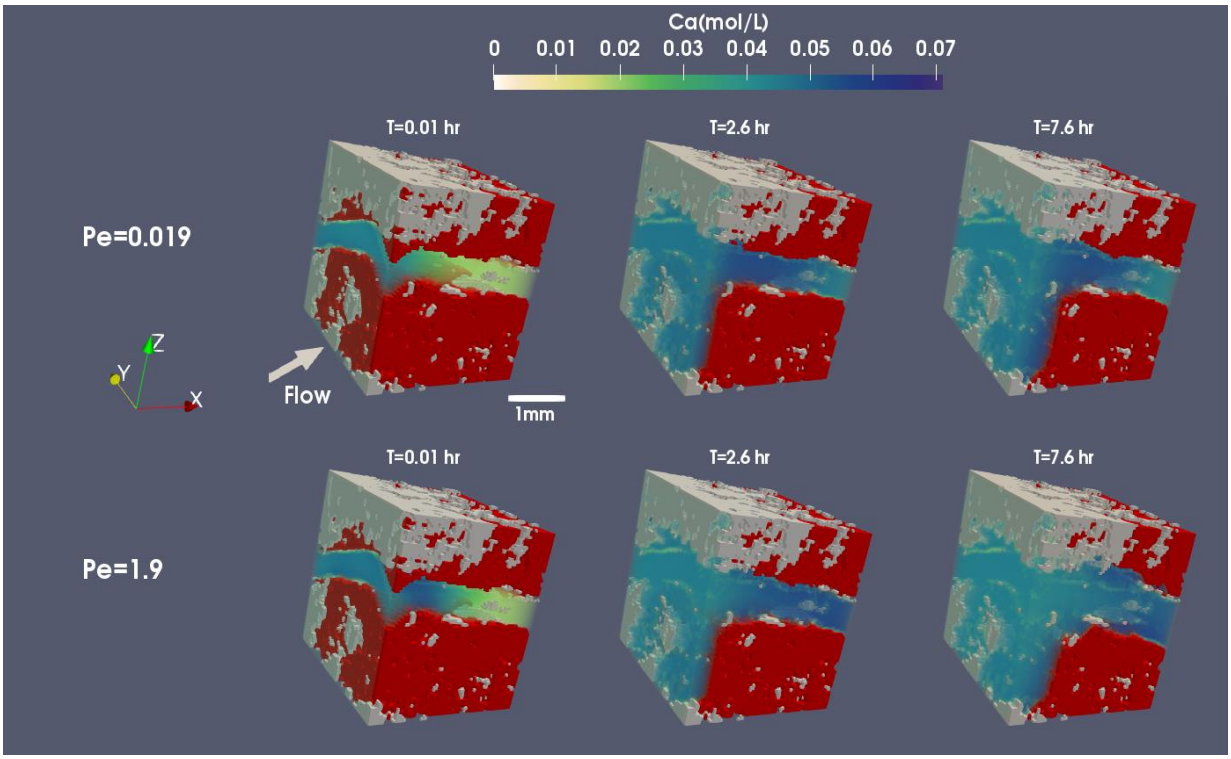

Figure 1. Ca concentration profile at t = 0.01 hr, t = 2.6 hr, and t = 7.6 hr. Upper panel corresponds to the lower injection rate and lower panel is related to the higher injection rate. In the figures red color is showing calcite and the gray coloration refers to nonreactive minerals.

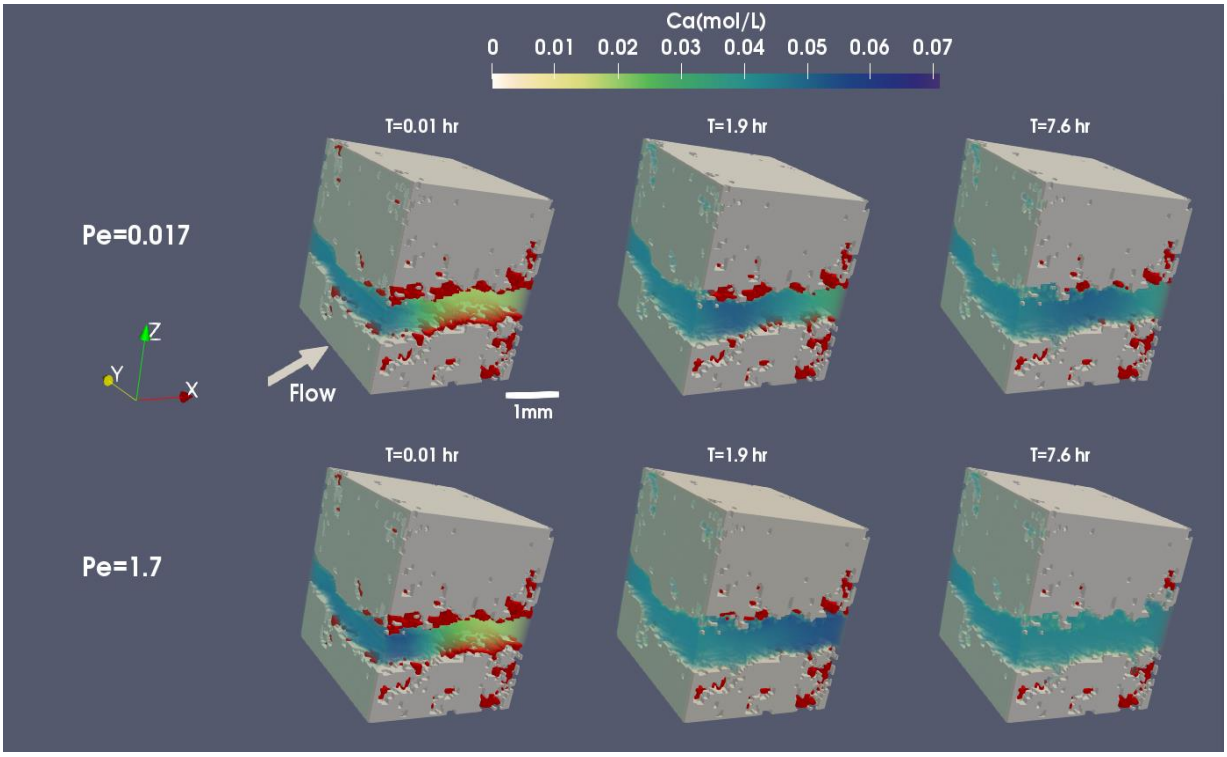

Figure 2. Ca concentration profile at t = 0.01 hr, t = 1.9 hr, and t = 7.6 hr. Upper panel corresponds to the lower injection rate and lower panel is related to the higher injection rate. In the figures red color is showing calcite and the gray coloration refers to nonreactive minerals.

185

186

187 **3.2.calcite dissolution rate**

188 In order to explore the effect of presence of nonreactive minerals on the bulk dissolution rate, the
189 effluent Ca concentration corresponding to Figures 1 and 2 have been plotted in Figures 3(a) and
190 3(b). We see here that Ca concentration initially increases until it reaches a maximum and then
191 decreases as the injection of low pH solution continues. This shows the overall rate of calcite
192 dissolution along the fracture decreased over time which confirms similar observations from
193 previous experimental works[6, 23, 39-40]. When the CO_2-rich brine is injected into the fractured
194 rock, it dissolves calcite and the dissolution rate is higher at the early stages of the simulation. As

the calcite along the fracture face dissolves, a calcite-depleted zone forms adjacent to the main flow path. Mass transport in these calcite-depleted regions is diffusion-limited meaning that less calcite is accessible to the low pH influent. This leads to greater buffering of pore fluid pH in the calcite-depleted zones, which subsequently causes a decrease in the rate of calcite dissolution.

Figure 3(a) indicates that when the calcite content along the fracture path is higher, the Ca concentration in the effluent is lower for slower flow rates. Some experimental studies showed similar results where they observed lower Ca concentrations for slower flow rates[40]. On the other hand, there are modeling studies[23] which showed a different trend where the Ca concentrations were higher for the slower flow rates. This behavior was attributed to the fact that when the flow rate is higher, the calcite-depleted zone forms more uniformly along the flow path. This means that pH buffering is observed in more areas along the fracture channel which is triggered by the diffusion limitation in the altered layer. When the flow rate is slower, the acidic solution flows more slowly and most of calcite dissolution occurs near the inlet and the calcite-depleted zone is therefore more localized close to the inlet. Hence, in the downstream areas where there is not any altered layer formed, there are still more accessible calcite surfaces close to the fracture face which can react with the low pH solution resulting in greater Ca release. However, as shown in Figure 3(a), in this case the behavior is opposite to prior works[23] with higher Ca concentrations observed at the higher flow rate. This opposite trend is due to the calcite distribution along the fracture channel. As is evident in Figure S3(d), the calcite volume fraction in the geometry increases as we move from the inlet towards the outlet. This prevents formation of an altered layer after dissolution of calcite in the regions near the outlet, which translates into a reduction in pH buffering in these areas since the transport regime is not diffusion-limited. All these characteristics allow for greater access of the reactive fluid to

218 additional calcite close to the outlet even at the higher flowrates; thus, higher Ca concentrations
219 are observed in the effluent due to more extensive dissolution.
220 Examination of the Ca concentration evolution for the low calcite simulations (Figure
221 3(b)) demonstrates a similar behavior to that shown in Figure 3(a). However, for the low calcite
222 case the difference in Ca concentration between the higher velocity and lower velocity
223 simulations is less than that for the case of high calcite content. Furthermore, Ca release was
224 greater at longer times for the slower flow rate (compared to higher flow rate) when calcite was
225 less abundant in the model domain. In the low calcite scenario, higher flow velocity results in a
226 faster breakthrough of dissolved Ca and leads to a higher peak in Ca concentration compared to
227 the slower injection scenario. At later simulation times, however, most of the available calcite in
228 the system has been dissolved and Ca concentration decreases. At slower flow rates, calcite
229 remains available near the fracture face and continues to dissolve at later times (especially at the
230 outlet as shown in Figure 2). This results in greater Ca concentration values (at later simulation
231 times) for slower flow rates compared to the high injection rate scenario.
232 Figures 3(a) and 3(b) also show that the Ca concentration in all scenarios approaches near steady
233 state. This is more evident in Figure 3(b) in which most of the calcite has been dissolved but in
234 Figure 3(a) where there are still more calcite available in the system changes might occur during
235 the later times of simulation.
236
237
238
239
240

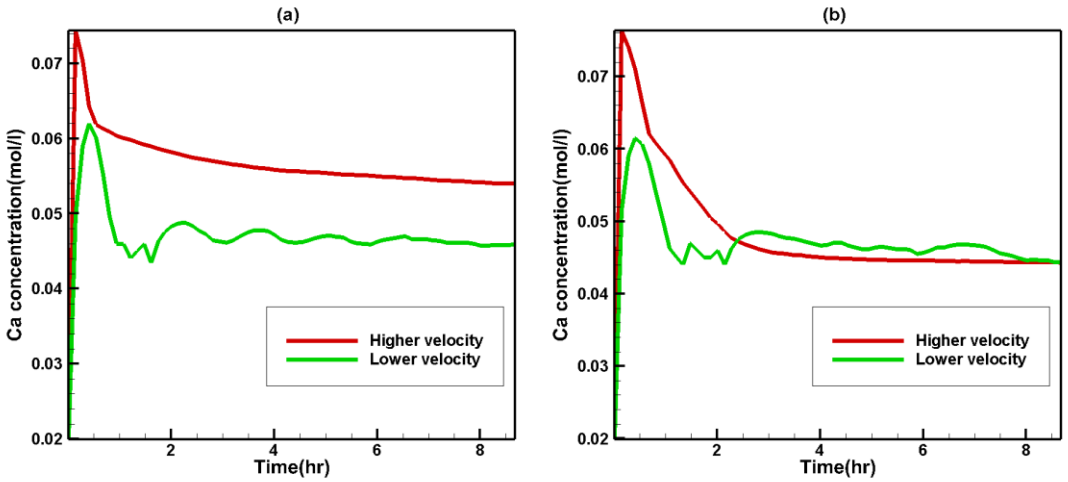

Figure 3. Comparison of Ca concentration at the outlet areas of the geometry with (a) high calcite content and (b) low calcite content at two different injection rates.

3.3. Porosity and permeability evolution

The dissolution of calcite leads to an increase in porosity and permeability of the fractured rock. The evolution of normalized permeability (permeability divided by initial permeability) and normalized porosity (porosity divided by initial porosity) are plotted in Figure 4 for both fracture geometries with high and low calcite content. As is evident in Figure 4, the evolution and rate of change in permeability is different depending on the injection velocities. Generally, for the higher fluid flow rates, the permeability increase is more pronounced compared to the case with lower velocity. As discussed in section 3.1, when the velocity is higher, the aperture increase mainly occurs along the fracture plane and consequently, this translates into a greater increase in fracture permeability. However, for the slower flow rate, less dissolution occurs further down the fracture due to the rapid buffering of the injected fluid near the inlet. Therefore, the aperture increase is more localized near the inlet when the injection rate is slow and increased porosity

due to calcite dissolution does not result in a substantial increase in fracture permeability compared to the case with higher injection velocity.

The other observed behavior in permeability evolution is that it increases until it reaches a plateau, which may be representative of the potential permeability increase due to calcite dissolution in a mineralogically heterogeneous rock (Figure 4). In continuum scale models in order to include the effects of reactions on the hydrodynamic properties of the fractured media, we need to relate porosity changes (calculated based on mineral mass from chemical calculations) to changes in permeability. Porosity driven changes to fracture permeability are usually assumed to follow a power law relationship, $\frac{k}{k_0} = (\frac{\varphi}{\varphi_0})^a$, in which k and φ are permeability and porosity with subscript zero indicating the initial values. The exponent, a, is most often assumed to be 3[41-44]. This cubic relation is valid if the fracture walls are smooth and parallel. Previous pore-scale simulations have confirmed that this cubic relation is valid for systems containing a fracture having smooth and parallel walls while surrounded by mono-mineral rock matrices[29, 35, 45]. These studies have also indicated that the porosity-permeability relationship may deviate from the cubic trend under different reaction and transport conditions but still they have a power law behavior[29, 35, 45]. The simulations performed in our work, however, show that the porosity-permeability relationship will not follow a power law relation. At longer simulation times when more calcite dissolves, model results demonstrate that fracture permeability begins to approach a constant value even as porosity continues to increase due to calcite dissolution. This behavior is clearer in Figure 4(d), which corresponds to the low calcite content case where most of calcite has been dissolved during the time scale of the simulations.

The deviation from a power law permeability-porosity relationship observed in Figure 4 may be attributed to the non-smooth fracture in the system and presence of nonreactive minerals in

the matrix. To investigate the effect of smoothness of the fracture on porosity and permeability evolution, we performed a simulation on the fracture geometry with high calcite content where all nonreactive minerals were replaced with calcite. Simulation results from this mono-mineralogical scenario (Figure S10) displayed a normalized porosity-permeability relation that did not show a power law relation. This confirms that when the fracture wall is non-smooth, the porosity-permeability relationship will not follow a power law trend. Figure S10 also compares the porosity and permeability evolution for the case containing nonreactive minerals with the case containing only calcite. This comparison indicates that the presence of nonreactive minerals in the rock matrix results in lower permeability increase for a given amount of porosity increase due to creation of porous and tortuous zones around the fracture. Figure S10 shows that the difference in permeability evolution between mono- and multi-mineral cases becomes more visible as more calcite is dissolved. This indicates that the negative effect on permeability enhancement, caused by presence of nonreactive minerals, is more pronounced at the later times of simulation.

Figures 4(c) and 4(d) at t= 11 hr show that for lower and higher velocity cases, the permeability values are the same (Figure 4(d)) but the porosities are not (Figure 4(c)). The larger porosities observed in the higher velocity scenario can be attributed to the dissolution of the calcite from the mixed mineral matrix adjacent to the fracture pathway. Although this dissolution results in increased porosity, a majority of this new porosity is within the rock matrix and does not contribute to the permeability enhancement and that is why same permeability values are observed.

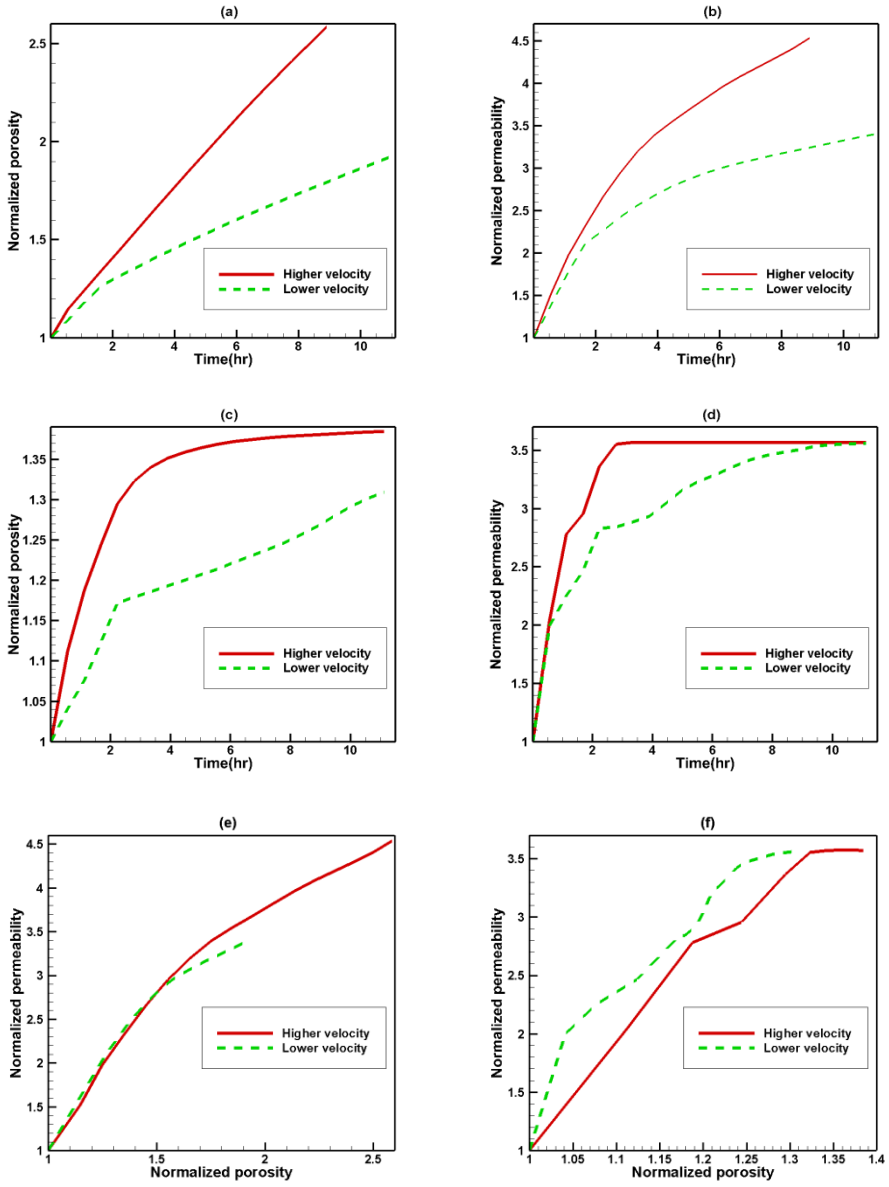

Figure 4. Plots (a) and (c) show normalized porosity vs time for geometries with high and low calcite content, respectively. Plots (b) and (d) display normalized permeability vs time for the geometry with high calcite and low calcite content, respectively. Normalized permeability vs normalized porosity are indicated in (e) and (f) for geometries with high and low calcite content, respectively. Normalized permeability is defined as permeability divided by initial permeability and normalized porosity is equal to porosity divided by initial porosity.

In figure 4(f) the normalized permeability, at a given normalized porosity, is higher for the lower velocity case. In the lower velocity case, it takes more time to reach a specific normalized porosity compared to the higher velocity case where it takes less time to have the same normalized porosity. For example, for the lower velocity case, it takes 7.7 hr to reach the normalized porosity of 1.24, while for the higher velocity we see normalized porosity of 1.24 at 1.6 hr. At t=7.7 hr (for the lower velocity case), calcite dissolution is greater compared to the calcite dissolution at t=1.6 hr (for the higher velocity case) even along the flow direction. This causes a higher permeability for the lower velocity case. Previous studies reported different results showing higher permeability for higher injection rates but those works were related to 2D simulations[46] or 3D simulations[47] for non-fractured media which might be the reason for having different results compared to our simulations.

3.4. 2D versus 3D simulations

3D simulations performed in this study account for the topographical features of the fracture and areal changes in aperture in addition to the mass transfer between the fracture and rock matrix. These are the features which were not simultaneously present in previously developed one and two dimensional models used to simulate fracture evolution during mineral dissolution[12, 29, 48-49]. 1D models can be used as a simple and computationally efficient modeling approach to simulate large domains and long time-scales and can provide insight regarding the important interplay between physical processes such as mineral dissolution and mass transfer[33]. However, such 1D models are unable to capture 2D variation in parameters such as fracture aperture along the fracture plane. These variations have been simulated using some 2D models that consider areal aperture changes in the fracture plane[12, 23, 49-50]. However, in these 2D models processes such as

fracture-matrix mass transfer are not included. There are other categories of 2D models which consider the mass transfer between fracture and matrix but lack the inclusion of areal topographical variations[29, 35]. 3D models are the most sophisticated approach to modeling flow through porous or fractured media but these models are usually computationally expensive, especially if one does not want to simplify the model chemistry. One possible option that can reduce this bottleneck might be to run several 2D simulations (with each having a 2D geometry along the flow direction and perpendicular to fracture plane) across the fracture plane and then taking the average behavior of the simulations as being most representative of 3D model system. To this end we selected nine different 2D-slices (along the flow direction and perpendicular to the fracture plane) from each 3D geometry with low and high calcite content and then injected the acidified brine into these 2D domains at both the low and high injection rates.

Figure 5 compares calcite dissolution for layer 50 from 3D simulation with the calcite dissolution for the same layer as investigated with 2D simulation. As is evident from Figure 5, the discrepancy between 2D and 3D simulations is not very large. When calcite content is high, the discrepancy between 2D and 3D simulations is smaller for the low injection rate scenario. For the case with lower calcite content, however, the calcite dissolution patterns are similar for both high and low injection rate because of the low amount of calcite initially present in the domain. When injection flow rate is high, all of this low calcite mass will be dissolved quickly leading to similar calcite dissolution patterns for the case of low calcite content even when flow rate is high. The dissolution pattern for the different layers can be seen in Figures S11-S18. The similarity between 2D and 3D simulations shows that it could be plausible to run a set of 2D simulations and then obtain the porosity and permeability evolution curves for different 2D layers and then average the results to obtain an equivalent porosity and permeability evolution

curve for the 3D geometry. Figures S19-S22 indicate the data points related to the porosity and permeability evolution for different 2D simulations (for different layers) and also the porosity and permeability evolution curve for the 3D simulation. It should be mentioned that a simple arithmetic average of 2D simulations cannot produce the porosity and permeability evolution curve of the 3D simulation since in the 3D simulations the presence of less tortuous zones will make it easier for the fluid to flow in these regions and hence, when averaging theses layers, the permeability in these layers should have a different weight.

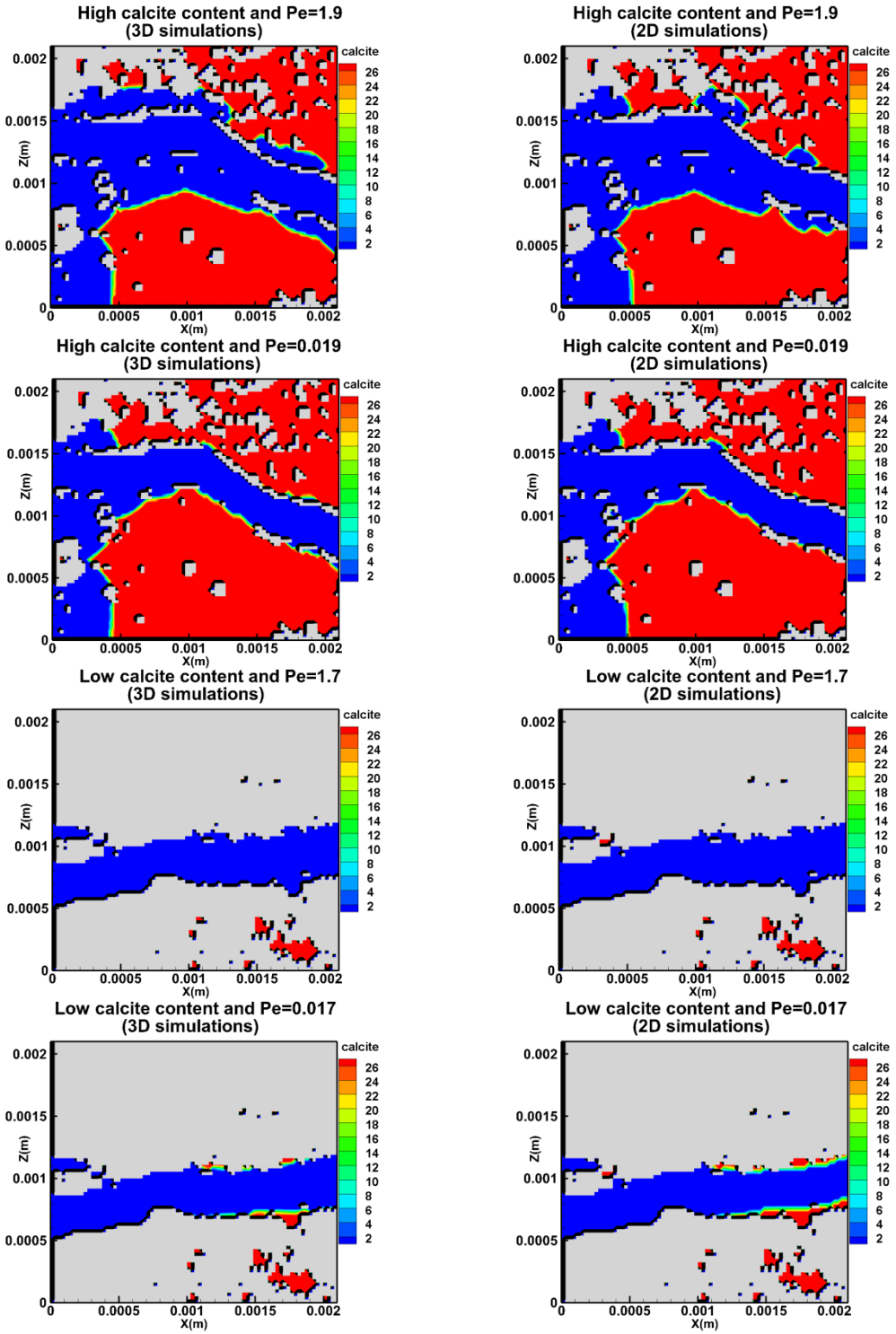

Figure 5. calcite mass (mol/L) for layer 50 at time = 8.3 hr. The left panels are related to the 3D simulations and right panels correspond to the 2D simulations.

4. Environmental Implications

Fractures are the main leakage pathways in the caprocks of CO_2 storage sites. It is therefore important to predict how their hydrodynamic properties change when their constituting minerals are in contact with CO_2-acidified brine. In this regard, pore-scale models, resolving processes at small scales, can play an important role to shed light on how factors such as mineral heterogeneity can affect the porosity and permeability of the fractures in the seals. By using a novel pore-scale model, this study has demonstrated that the co-existence of minerals with vastly different reactivities can lead to formation of porous layers around the main fracture, a finding that confirms previous experimental and numerical studies reporting formation of this layer[7, 10, 22-24, 29, 40, 49]. Results showed that the overall calcite dissolution rate decreases as the altered layer forms around the fracture. This is similar to the findings in previous experimental studies[6, 23, 39] performed on heterogeneous carbonate rocks. Moreover, injection of acidic fluid at different flow rates indicated that at lower flow rates, overall dissolution rate becomes slower which is consistent with results obtained in prior experimental works[40]. Plotting the normalized permeability vs normalized porosity indicated that the altered layer can restrict the increase in fracture permeability along a dissolving fracture. This behavior also confirms the porosity-permeability relations reported in previous studies[29]. The porosity-permeability relations obtained here show that the general cubic law, which is most applicable for mineralogically homogeneous smooth fractures in large models, is not valid for multi-mineral fractured systems. Using these types of simplified porosity-permeability relationships in large scale models may thus lead to an overestimation in increased fracture permeability for a given increase in porosity.

At reservoir scales, where fractured rocks may be modeled as discrete fractures, alteration of properties of individual fractures should be properly modeled[24]. The pore-scale model presented

in this study can be used as a tool to provide inputs to reservoir scale models such as improved porosity-permeability relationships. In the context of caprock integrity, the pore scale model can be used to better simulate the transport processes involved in CO_2 leakage in fractured seals where the spatial distribution of different reactive minerals are known through use of various imaging techniques.

At the reservoir scale, there is a need for more computationally efficient models[49]. Comparison of calcite dissolution patterns for different layers in 2D and 3D simulations in our work showed that one might perform several 2D simulations (with different 2D layers, along the fracture and perpendicular to the fracture plane, as input geometry for 2D simulations) instead of one 3D simulation. This may serve to reduce the computational challenges associated with 3D pore scale simulations while still, within uncertainty, achieve the same qualitative and quantitative results as the full 3D simulations.

In this study we treated all non-calcite minerals as non-reactive given the short time scale of the simulations. In the longer time scales, other slow reacting minerals can be treated as reactive. In that case, the evolution of fracture geometry and its hydrodynamic properties might be more complex as there may be secondary precipitation triggered by dolomite reaction as seen by previous studies[51] (for non-fractured media).

ASSOCIATED CONTENT

Supporting Information

The supporting information is available free of charge.

The details of the Lattice Boltzmann model for fluid flow and species transport equations; table summarizing influent and initial concentrations; table listing initial fracture porosity and permeability; fracture aperture and calcite content maps; figures showing the initial Ca and pH profiles; figures indicating temporal evolution of pH; plots comparing normalized porosity and normalized permeability values for multi-mineral and mono-mineral cases; Figures indicating the calcite dissolution pattern for different layers of 3D geometry obtained by performing 3D and 2D simulations; and figures showing the temporal evolution of porosity and permeability for 3D simulation as well as 2D simulations for different layers of 3D geometry.

AUTHOR INFORMATION

Corresponding Author

*Email: Hossein.Fazeli@geo.uio.no

ACKNOWLEDGMENT

H. Fazeli and H. Hellevang acknowledge the funding received for this study from PROTECT project (No. 233736) financed by the Research Council of Norway, Total E&P and Dea. R. Patel acknowledges the funding received for this study from the European union's Horizon 2020 research and innovation programme under the Marie Sklodowska-Curie grant agreement No 701647.

REFERENCES

1. Bui, M.; Adjiman, C. S.; Bardow, A.; Anthony, E. J.; Boston, A.; Brown, S.; Fennell, P. S.; Fuss, S.; Galindo, A.; Hackett, L. A., Carbon capture and storage (CCS): the way forward. *Energy & Environmental Science* **2018,** *11* (5), 1062-1176.
2. Change, I. P. o. C., *Climate change 2014: mitigation of climate change*. Cambridge University Press: 2015; Vol. 3.
3. Hellevang, H., Carbon capture and storage (CCS). In *Petroleum Geoscience*, Springer: 2015; pp 591-602.
4. Berkowitz, B., Characterizing flow and transport in fractured geological media: A review. *Advances in water resources* **2002,** *25* (8-12), 861-884.
5. Carroll, S.; Carey, J. W.; Dzombak, D.; Huerta, N. J.; Li, L.; Richard, T.; Um, W.; Walsh, S. D.; Zhang, L., Role of chemistry, mechanics, and transport on well integrity in CO2 storage environments. *International Journal of Greenhouse Gas Control* **2016,** *49*, 149-160.
6. Deng, H.; Voltolini, M.; Molins, S.; Steefel, C.; DePaolo, D.; Ajo-Franklin, J.; Yang, L., Alteration and erosion of rock matrix bordering a carbonate-rich shale fracture. *Environmental science & technology* **2017,** *51* (15), 8861-8868.
7. Ellis, B.; Peters, C.; Fitts, J.; Bromhal, G.; McIntyre, D.; Warzinski, R.; Rosenbaum, E., Deterioration of a fractured carbonate caprock exposed to CO2-acidified brine flow. *Greenhouse Gases: Science and Technology* **2011,** *1* (3), 248-260.
8. Kampman, N.; Bickle, M.; Wigley, M.; Dubacq, B., Fluid flow and CO2–fluid–mineral interactions during CO2-storage in sedimentary basins. *Chemical Geology* **2014,** *369*, 22-50.
9. Zhang, L.; Soong, Y.; Dilmore, R.; Lopano, C., Numerical simulation of porosity and permeability evolution of Mount Simon sandstone under geological carbon sequestration conditions. *Chemical Geology* **2015,** *403*, 1-12.
10. Ellis, B. R.; Peters, C. A., 3D Mapping of calcite and a demonstration of its relevance to permeability evolution in reactive fractures. *Advances in water resources* **2016,** *95*, 246-253.
11. Detwiler, R. L.; Glass, R. J.; Bourcier, W. L., Experimental observations of fracture dissolution: The role of Peclet number on evolving aperture variability. *Geophysical Research Letters* **2003,** *30* (12), 1648-1651.
12. Elkhoury, J. E.; Ameli, P.; Detwiler, R. L., Dissolution and deformation in fractured carbonates caused by flow of CO2-rich brine under reservoir conditions. *International Journal of Greenhouse Gas Control* **2013,** *16*, S203-S215.
13. Starchenko, V.; Marra, C. J.; Ladd, A. J., Three-dimensional simulations of fracture dissolution. *Journal of Geophysical Research: Solid Earth* **2016,** *121* (9), 6421-6444.
14. Szymczak, P.; Ladd, A., Microscopic simulations of fracture dissolution. *Geophysical research letters* **2004,** *31* (23), L23606 (1-4).
15. Szymczak, P.; Ladd, A., A network model of channel competition in fracture dissolution. *Geophysical Research Letters* **2006,** *33* (5), L05401 (1-4).
16. Szymczak, P.; Ladd, A., Wormhole formation in dissolving fractures. *Journal of Geophysical Research: Solid Earth* **2009,** *114* (B6), B06203 (1-22).
17. Szymczak, P.; Ladd, A. J., The initial stages of cave formation: Beyond the one-dimensional paradigm. *Earth and Planetary Science Letters* **2011,** *301* (3-4), 424-432.
18. Szymczak, P.; Ladd, A. J., Reactive-infiltration instabilities in rocks. Fracture dissolution. *Journal of Fluid Mechanics* **2012,** *702*, 239-264.

19. Upadhyay, V. K.; Szymczak, P.; Ladd, A. J., Initial conditions or emergence: What determines dissolution patterns in rough fractures? *Journal of Geophysical Research: Solid Earth* **2015,** *120* (9), 6102-6121.
20. Verberg, R.; Ladd, A., Simulation of chemical erosion in rough fractures. *Physical Review E* **2002,** *65* (5), 056311.
21. Noiriel, C.; Madé, B.; Gouze, P., Impact of coating development on the hydraulic and transport properties in argillaceous limestone fracture. *Water resources research* **2007,** *43* (9), W09406 (1-16).
22. Deng, H.; Ellis, B. R.; Peters, C. A.; Fitts, J. P.; Crandall, D.; Bromhal, G. S., Modifications of carbonate fracture hydrodynamic properties by CO2-acidified brine flow. *Energy & Fuels* **2013,** *27* (8), 4221-4231.
23. Deng, H.; Molins, S.; Steefel, C.; DePaolo, D.; Voltolini, M.; Yang, L.; Ajo-Franklin, J., A 2.5 D reactive transport model for fracture alteration simulation. *Environmental science & technology* **2016,** *50* (14), 7564-7571.
24. Deng, H.; Steefel, C.; Molins, S.; DePaolo, D., Fracture evolution in multimineral systems: The role of mineral composition, flow rate, and fracture aperture heterogeneity. *ACS Earth and Space Chemistry* **2018,** *2* (2), 112-124.
25. Spokas, K.; Peters, C. A.; Pyrak-Nolte, L., Influence of Rock Mineralogy on Reactive Fracture Evolution in Carbonate-Rich Caprocks. *Environmental science & technology* **2018,** *52* (17), 10144-10152.
26. Liu, M.; Shabaninejad, M.; Mostaghimi, P., Impact of mineralogical heterogeneity on reactive transport modelling. *Computers & Geosciences* **2017,** *104*, 12-19.
27. Liu, M.; Shabaninejad, M.; Mostaghimi, P., Predictions of permeability, surface area and average dissolution rate during reactive transport in multi-mineral rocks. *Journal of Petroleum Science and Engineering* **2018,** *170*, 130-138.
28. Min, T.; Gao, Y.; Chen, L.; Kang, Q.; Tao, W.-w., Changes in porosity, permeability and surface area during rock dissolution: Effects of mineralogical heterogeneity. *International Journal of Heat and Mass Transfer* **2016,** *103*, 900-913.
29. Chen, L.; Kang, Q.; Viswanathan, H. S.; Tao, W. Q., Pore-scale study of dissolution-induced changes in hydrologic properties of rocks with binary minerals. *Water Resources Research* **2014,** *50* (12), 9343-9365.
30. Molins, S.; Trebotich, D.; Miller, G. H.; Steefel, C. I., Mineralogical and transport controls on the evolution of porous media texture using direct numerical simulation. *Water Resources Research* **2017,** *53* (5), 3645-3661.
31. Charlton, S. R.; Parkhurst, D. L., Modules based on the geochemical model PHREEQC for use in scripting and programming languages. *Computers & Geosciences* **2011,** *37* (10), 1653-1663.
32. Michael, K.; Golab, A.; Shulakova, V.; Ennis-King, J.; Allinson, G.; Sharma, S.; Aiken, T., Geological storage of CO 2 in saline aquifers—a review of the experience from existing storage operations. *International Journal of Greenhouse Gas Control* **2010,** *4* (4), 659-667.
33. Fitts, J. P.; Peters, C. A., Caprock fracture dissolution and CO2 leakage. *Reviews in Mineralogy and Geochemistry* **2013,** *77* (1), 459-479.
34. Patel, R. A.; Perko, J.; Jacques, D.; De Schutter, G.; Van Breugel, K.; Ye, G., A versatile pore-scale multicomponent reactive transport approach based on lattice Boltzmann method: Application to portlandite dissolution. *Physics and Chemistry of the Earth, Parts A/B/C* **2014,** *70*, 127-137.

35. Fazeli, H.; Patel, R.; Hellevang, H., Effect of Pore-Scale Mineral Spatial Heterogeneity on Chemically Induced Alterations of Fractured Rock: A Lattice Boltzmann Study. *Geofluids* **2018,** *2018*, 1-28.
36. Palandri, J. L.; Kharaka, Y. K. *A compilation of rate parameters of water-mineral interaction kinetics for application to geochemical modeling*; Geological Survey Menlo Park CA: 2004.
37. Chou, L.; Garrels, R. M.; Wollast, R., Comparative study of the kinetics and mechanisms of dissolution of carbonate minerals. *Chemical geology* **1989,** *78* (3-4), 269-282.
38. Plummer, L.; Wigley, T.; Parkhurst, D., The kinetics of calcite dissolution in CO 2-water systems at 5 degrees to 60 degrees C and 0.0 to 1.0 atm CO 2. *American journal of science* **1978,** *278* (2), 179-216.
39. Ajo-Franklin, J.; Voltolini, M.; Molins, S.; Yang, L., Coupled processes in a fractured reactive system: A dolomite dissolution study with relevance to gcs caprock integrity. *Geological Carbon Storage: Subsurface Seals and Caprock Integrity* **2018,** *238*, 187.
40. Ellis, B. R.; Fitts, J. P.; Bromhal, G. S.; McIntyre, D. L.; Tappero, R.; Peters, C. A., Dissolution-driven permeability reduction of a fractured carbonate caprock. *Environmental engineering science* **2013,** *30* (4), 187-193.
41. Steefel, C.; Appelo, C.; Arora, B.; Jacques, D.; Kalbacher, T.; Kolditz, O.; Lagneau, V.; Lichtner, P.; Mayer, K. U.; Meeussen, J., Reactive transport codes for subsurface environmental simulation. *Computational Geosciences* **2015,** *19* (3), 445-478.
42. Steefel, C. I.; Lasaga, A. C., A coupled model for transport of multiple chemical species and kinetic precipitation/dissolution reactions with application to reactive flow in single phase hydrothermal systems. *American Journal of science* **1994,** *294* (5), 529-592.
43. Hommel, J.; Coltman, E.; Class, H., Porosity–Permeability Relations for Evolving Pore Space: A Review with a Focus on (Bio-) geochemically Altered Porous Media. *Transport in Porous Media* **2018,** *124* (2), 589-629.
44. Zimmerman, R. W.; Bodvarsson, G. S., Hydraulic conductivity of rock fractures. *Transport in porous media* **1996,** *23* (1), 1-30.
45. Liu, M.; Mostaghimi, P., Pore-scale modelling of CO 2 storage in fractured coal. *International Journal of Greenhouse Gas Control* **2017,** *66*, 246-253.
46. Kang, Q.; Chen, L.; Valocchi, A. J.; Viswanathan, H. S., Pore-scale study of dissolution-induced changes in permeability and porosity of porous media. *Journal of hydrology* **2014,** *517*, 1049-1055.
47. Liu, M.; Mostaghimi, P., Characterisation of reactive transport in pore-scale correlated porous media. *Chemical Engineering Science* **2017,** *173*, 121-130.
48. Steefel, C. I.; Lichtner, P. C., Multicomponent reactive transport in discrete fractures: I. Controls on reaction front geometry. *Journal of Hydrology* **1998,** *209* (1-4), 186-199.
49. Deng, H.; Fitts, J. P.; Crandall, D.; McIntyre, D.; Peters, C. A., Alterations of fractures in carbonate rocks by CO2-acidified brines. *Environmental science & technology* **2015,** *49* (16), 10226-10234.
50. Spokas, K.; Peters, C. A.; Pyrak-Nolte, L., The Influence of Rock Mineralogy on Reactive Fracture Evolution in Carbonate-rich Caprocks. *Environmental science & technology* **2018,** *52* (17), 10144-10152.
51. Kang, Q.; Lichtner, P. C.; Viswanathan, H. S.; Abdel-Fattah, A. I., Pore scale modeling of reactive transport involved in geologic CO2 sequestration. *Transport in porous media* **2010,** *82* (1), 197-213.

614

615 GRAPHICAL ABSTRACT

616